INTERNATIONAL JOURNAL FOR NUMERICAL METHODS IN FLUIDS
Int. J. Numer. Meth. Fluids 2008; **57**:157–176
Published online 11 October 2007 in Wiley InterScience (www.interscience.wiley.com). DOI: 10.1002/fld.1625

The characteristic-based split (CBS) scheme for viscoelastic flow past a circular cylinder

Chun-Bin Liu and P. Nithiarasu*, †

School of Engineering, Swansea University, Swansea SA2 8PP, U.K.

SUMMARY

A fully explicit, characteristic-based split (CBS) method for viscoelastic flow past a circular cylinder, placed in a rectangular channel, is presented. The pressure equation in its explicit form is employed *via* an artificial compressibility parameter. The constitutive equations used here are based on the Oldroyd-B model. No loss of convergence to steady state was observed in any of the results presented in this paper. Comparison of the present results with other available numerical data shows that the CBS algorithm is in excellent agreement with them at lower Deborah numbers. However, at higher Deborah numbers, the present results differ from other numerical solutions. This is due to the fact that the positive definitiveness of the conformation matrix is lost between a Deborah number of 0.6 and 0.7. However, the positive definitiveness is retained when an artificial diffusion is added to the discrete constitutive equations at higher Deborah numbers. It appears that the fractional solution stages used in the CBS scheme and the higher-order time step-based convection stabilization clearly reduce the instability at higher Deborah numbers. The Deborah number limit reached in the present work is three without artificial dissipation and two with artificial dissipation. Copyright © 2007 John Wiley & Sons, Ltd.

Received 3 June 2007; Revised 26 August 2007; Accepted 29 August 2007

KEY WORDS: CBS scheme; artificial compressibility (AC); Oldroyd-B; artificial dissipation; FEM; fractional step

1. INTRODUCTION

Mathematical representation of viscoelastic flows is often expressed by differential type, hyperbolic, constitutive equations. Many currently available numerical solution procedures for such

*Correspondence to: P. Nithiarasu, School of Engineering, Swansea University, Swansea SA2 8PP, U.K.
†E-mail: P.Nithiarasu@swansea.ac.uk

Contract/grant sponsor: Engineering and Physical Sciences Research Council (EPSRC); contract/grant number: EP/C515498/1

flows are subjected to strong instability, especially at higher Deborah numbers. It is also obvious from the available literature that obtaining mesh convergence and convergence to steady state is extremely difficult at higher Deborah numbers.

The mixed finite element algorithms have been dominating the viscoelastic flow modelling over the last two decades [1]. Numerical stability of such schemes has been the focus of many studies, especially at higher fluid elasticity. Some of the attempts to stabilize viscoelastic flow calculations include elastic viscous split formulation (EVSS) [2, 3], explicitly elliptic momentum equations (EEME) [4, 5], EVSS-G method [6] with an independent interpolation for velocity gradients, adaptive EVSS [7], discrete EVSS (DEVSS) formulation [8], discrete EVSS-G method [9, 10] and DAVSS-ω formulation [11].

Majority of the reported work, using the Oldroyd-B model for flow past a circular cylinder, at higher Deborah numbers (*De*), suffers from loss of convergence to steady state on fine meshes. Phan-Thien and Dou [11–13] identified that the solution exhibits stress oscillations in the wake along with large values of primary (first) normal stress difference at the front stagnation point of a cylinder. Fan *et al.* [14] suggested that the solutions resulted from the higher *De* may be numerical artefacts. Fan also indicated a lack of convergence of the solution beyond a *De* of 0.7. Coronado *et al.* [15] further explained that around $De=0.7$ the conformation tensor loses its positive definiteness due to the sharp stress boundary layer developed on the cylinder surface. It was shown by Caola *et al.* [16] that reaching a steady state beyond a *De* of unity is difficult. This is due to the linear increase in the extra stress at the rear stagnation point. Alves *et al.* [17] and Hulsen *et al.* [18] argued that the normal, extra stress variation in the wake of the cylinder resulted in numerical divergence. Recently, Kim *et al.* [19] refined grids along the centreline and found a singular behaviour of extra stresses at higher Deborah numbers in the wake region. In summary, majority of the proposed methods have some form of stability problem beyond a Deborah number of unity.

Fractional step methods (often referred to as pressure or velocity correction method) are currently not very popular in the viscoelastic flow modelling. It is unclear why this method was considered unsuitable for complex geometries and complex flow problems [11]. Our past experience shows that these methods can be adopted to viscoelastic flow problems by incorporating appropriate modifications [20]. The instability in the momentum equation is often the subject of discussion by many previously published papers. It is known that the first-order convection, pressure and extra stress terms in the momentum equation are the sources of spatial instability in their discrete form if central type approximations are introduced. Another instability due to lack of pressure stabilization is often reduced by introducing different interpolation functions for pressure and velocity. Although this is an acceptable procedure, simplicity of equal order interpolation is lost. The classical fractional step method [21], however, reduces the pressure instability by splitting the equations into fractional stages and allows equal order interpolation. The classical fractional step methods are known to introduce a first-order time error in pressure [22–25]. However, this can be easily eliminated by suitable extra pressure stabilization [25, 26]. For steady-state problems, however, this is not an issue and classical fractional step method is sufficient. The instability due to the central-type spatial discretization of first-order terms in the momentum equation needs different treatments and a stabilized form for the momentum equation is needed. Here, instead of classical stabilization methods, we introduce a higher-order time stepping scheme *via* a characteristic-based approach to achieve stabilzation [27]. The higher-order terms not only act as a stablizing mechanism but also give a higher-order time accuracy. Since the method involves a split (fractional step) and a characteristic-Galerkin approximation, it is referred to as the characteristic-based split (CBS)

DOI: 10.1002/fld

method. Owing to the reasons cited above, the CBS scheme for viscoelastic flows can be stable subjected to obtaining a stable solution for constitutive equations.

Our experience shows that applying simple explicit characteristic-Galerkin method [27, 28] directly to the constitutive equations gives stable extra stress solutions up to a certain limiting Deborah or Weissenberg numbers [20]. Beyond this number, though fully converged solution can be obtained, the stress and pressure fields are normally marked with minor oscillations. The limiting *De*, we previously found, was approximately unity [20]. Beyond this value, addition of an extra discrete, artificial dissipation to the constitutive equations helps in the stabilization of spatial oscillations. However, there was no need for extra additional viscosities in the momentum equation. This again demonstrates that the fractional stage solution procedure eliminates the need for additional dissipation in the momentum equation. The artificial damping needed for the constitutive equation is often very small to obtain a smooth solution at lower Deborah numbers. However, at higher Deborah numbers the artificial damping may introduce its own extra drag component if such damping is arbitrarily added and thus can artificially enhance the predicted drag values. In our previous work [20], the extra dissipation helped to increase the Deborah number limit to a value above unity and we provided results up to a Deborah number value of 1.6. Beyond this value, although steady state was possible, the drag force was increasing uncontrollably due to the extra dissipation. Thus, in the present work, we establish the performance of the CBS method without and with adding additional damping. We add enough damping in a controlled manner just to retain the positive definitiveness of the conformation matrix.

Over the last 10 years, the CBS method has been evolved to unify the viscous compressible and incompressible flow calculations [20, 25, 28–40]. In the present paper, in addition to providing extension of the CBS scheme to general viscoelastic flows and using unstructured meshes to address the mesh convergence and related issues, we also provide a thorough analysis of the results obtained in the presence and absence of additional, artificial damping. The results are presented for a range of Deborah numbers between 0 and 3.

2. MATHEMATICAL FORMULATIONS

2.1. Governing equations

The non-dimensional isothermal fluid dynamics equations for viscoelastic flows in conservation form may be written as

$$\frac{\partial \mathbf{W}}{\partial t}+\frac{\partial \mathbf{F}_j}{\partial x_j}+\frac{\partial \mathbf{G}_j}{\partial x_j}=0 \tag{1}$$

where the variable vector is given as

$$\mathbf{W}=(\rho, \rho u_1, \rho u_2)^{\mathrm{T}} \tag{2}$$

The convective acceleration vector $\mathbf{F}_j$ in Equation (1) is defined as

$$\mathbf{F}_j=\left(\rho u_j, \frac{\delta_{1j}p}{Re}+\rho u_1 u_j, \frac{\delta_{2j}p}{Re}+\rho u_2 u_j\right)^{\mathrm{T}} \tag{3}$$

DOI: 10.1002/fld

The viscoelastic diffusion vector $\mathbf{G}$ in Equation (1) is given as

$$\mathbf{G}_j = \left(0, \frac{1}{Re}(-\tau_{1j}^n - \tau_{1j}^p), \quad \frac{1}{Re}(-\tau_{2j}^n - \tau_{2j}^p)\right)^{\mathrm{T}} \tag{4}$$

where the Newtonian deviatoric stress tensor in the above equation is

$$\tau_{ij}^n = (1-\alpha)\left(\frac{\partial u_i}{\partial x_j} + \frac{\partial u_j}{\partial x_i} - \frac{2}{3}\frac{\partial u_k}{\partial x_k}\delta_{ij}\right) \tag{5}$$

and the non-Newtonian deviatoric stress tensor is given by the constitutive equations of extra stresses, i.e.

$$\tau_{ij}^p = -De\left[\frac{\partial \tau_{ij}^p}{\partial t} + \frac{\partial}{\partial x_k}(u_k \tau_{ij}^p) - \tau_{ik}^p \frac{\partial u_j}{\partial x_k} - \tau_{jk}^p \frac{\partial u_i}{\partial x_k}\right] + \alpha\left(\frac{\partial u_i}{\partial x_j} + \frac{\partial u_j}{\partial x_i} - \frac{2}{3}\frac{\partial u_k}{\partial x_k}\delta_{ij}\right) \tag{6}$$

In the above governing equations, p is the pressure, ρ is the density, u_j are the velocity components, δ_{ij} is the Kronecker delta, $\alpha = \eta_{m0}/\eta_0$ in which η_{m0} represents the polymer-contributed viscosity and η_0 represents the zero shear rate viscosity, Re is the Reynolds number and De is the Deborah number defined as

$$Re = \frac{\rho_\infty u_\infty L}{\eta_0}; \quad De = \frac{\lambda u_\infty}{L} \tag{7}$$

where subscript ∞ indicates a free stream value, L is a characteristic length, λ is the relaxation time and $\eta_0 = \eta_n + \eta_{m0}$ in which η_n represents the Newtonian dynamic viscosity. When $0 < \alpha < 1$, the constitutive equation describes the Oldroyd-B model. The upper convected Maxwell (UCM) model is obtained when $\alpha = 1$. Some other viscoelastic fluid models may be found in [41–43].

2.2. CBS formulation

The CBS scheme is based on the characteristic-Galerkin procedure and a fractional step method [29, 38]. It is widely used to carry out fluid dynamic calculations. In this paper, fully explicit CBS-based artificial compressibility (CBS-AC) form has been employed to solve viscoelastic flow. Following the intermediate momentum at the first step, the pressure equation derived from the mass conservation is used at step 2. The velocity field is corrected at the third step. Finally, the constitutive equations are solved at the fourth step. The semi-discrete form of these steps is expressed

Step 1: Intermediate momentum

$$\begin{aligned}\Delta U_j^\star &= U_j^\star - U_j^n \\ &= \Delta t\left[-\frac{\partial}{\partial x_k}(u_k U_j) + \frac{1}{Re}\frac{\partial \tau_{ij}^n}{\partial x_i} + \frac{1}{Re}\frac{\partial \tau_{ij}^p}{\partial x_i}\right]^n \\ &\quad + \frac{(\Delta t)^2}{2}\left\{u_m \frac{\partial}{\partial x_m}\left[\frac{\partial}{\partial x_k}(u_k U_j) - \frac{1}{Re}\frac{\partial \tau_{ij}^p}{\partial x_i}\right]\right\}^n\end{aligned} \tag{8}$$

where $U_j^n = U_j(t_n) = \rho u_j^n$, $\Delta t = t^{n+1} - t^n$ and $\star$ indicates an intermediate quantity.

DOI: 10.1002/fld

Step 2: Pressure

$$\frac{1}{Re}\left(\frac{1}{c^2}\right)^n \Delta p \approx \frac{1}{Re}\left(\frac{1}{\beta^2}\right)^n (p^{n+1}-p^n)$$
$$= -\Delta t\left[\frac{\partial U_j^n}{\partial x_j}+\theta_1\frac{\partial \Delta U_j^\star}{\partial x_j}-\frac{\Delta t\theta_1}{Re}\left(\frac{\partial^2 p^n}{\partial x_j \partial x_j}+\theta_2\frac{\partial^2 \Delta p}{\partial x_j \partial x_j}\right)\right] \tag{9}$$

where c is the speed of sound which assumes that density changes are related to pressure changes for small compressibility or elastic deformability and approaches infinity for incompressible flows. However, the wave speed c can be replaced by an artificial compressibility parameter β to carry out incompressible flow calculations. For the explicit CBS-AC scheme, β depends on convective, diffusive and viscoelastic wave speeds, i.e.

$$\beta = \max(\varepsilon, u_{\text{conv}}, u_{\text{diff}}, u_{\text{visc}}) \tag{10}$$

where ε is a small number and is taken equal to 0.5 in the present study, $u_{\text{conv}} = \sqrt{u_i u_i}$, $u_{\text{diff}} = \frac{h}{2Re}$ and $u_{\text{visc}} = \sqrt{1/ReDe}$. The time step values are locally defined as

$$\Delta t = \frac{h}{u_{\text{conv}}+\beta} \tag{11}$$

More details on the time steps and artificial compressibility forms may be found in [20, 35, 38].

Step 3: Momentum correction

$$\Delta U_j = U_j^{n+1} - U_j^n$$
$$= \Delta U_j^\star - \frac{\Delta t}{Re}\frac{\partial p}{\partial x_j}^{n+\theta_2} + \frac{(\Delta t)^2}{2Re}u_m^n\frac{\partial^2 p^n}{\partial x_m \partial x_j} \tag{12}$$

where $0.5 \leqslant \theta_1 \leqslant 1$ and $\theta_2 = 0$ for explicit forms and $0.5 \leqslant \theta_1 \leqslant 1$ and $0.5 \leqslant \theta_2 \leqslant 1$ for semi-implicit forms. In this work, $\theta_1 = 1$ and $\theta_2 = 0$ are employed.

Step 4: Constitutive equation

$$\Delta\tau_{ij}^p = \tau_{ij}^{p\,n+1} - \tau_{ij}^{p\,n}$$
$$= \Delta t\left[-\frac{\partial}{\partial x_k}\left(u_k\tau_{ij}^p\right)-\frac{\tau_{ij}^p}{De}\right]^n$$
$$+\Delta t\left[\tau_{ik}^p\frac{\partial u_j}{\partial x_k}+\tau_{jk}^p\frac{\partial u_i}{\partial x_k}+\frac{\alpha}{De}\left(\frac{\partial u_i}{\partial x_j}+\frac{\partial u_j}{\partial x_i}-\frac{2}{3}\frac{\partial u_k}{\partial u_k}\delta_{ij}\right)\right]^n$$
$$+\frac{(\Delta t)^2}{2}\left\{u_m\frac{\partial}{\partial x_m}\left[\frac{\partial}{\partial x_k}(u_k\tau_{ij}^p)+\frac{\tau_{ij}^p}{De}\right]\right\}^n$$

DOI: 10.1002/fld

$$+\frac{(\Delta t)^2}{2}\left\{u_m\frac{\partial}{\partial x_m}\left[-\left(\tau_{ik}^p\frac{\partial u_j}{\partial x_k}+\tau_{jk}^p\frac{\partial u_i}{\partial x_k}\right)\right]\right\}^n$$
$$+\frac{(\Delta t)^2}{2}\left\{u_m\frac{\partial}{\partial x_m}\left[-\frac{\alpha}{De}\left(\frac{\partial u_i}{\partial x_j}+\frac{\partial u_j}{\partial x_i}-\frac{2}{3}\frac{\partial u_k}{\partial u_k}\delta_{ij}\right)\right]\right\}^n \tag{13}$$

The spatial discretizations of the variables are given as

$$\begin{aligned} &U_j=\mathbf{N}_u\tilde{\mathbf{U}}_j; \quad \Delta U_j=\mathbf{N}_u\Delta\tilde{\mathbf{U}}_j; \quad \Delta U_j^\star=\mathbf{N}_u\Delta\tilde{\mathbf{U}}_j^\star; \quad u_j=\mathbf{N}_u\tilde{\mathbf{u}}_j \\ &\Delta p=\mathbf{N}_p\Delta\tilde{\mathbf{p}}; \quad p=\mathbf{N}_p\tilde{\mathbf{p}}; \quad \tau_{ij}^p=\mathbf{N}_{\tau^p}\tilde{\boldsymbol{\tau}}_{ij}^p \end{aligned} \tag{14}$$

where $\mathbf{N}$ are the shape functions and $\tilde{}$ indicates a nodal quantity.

Applying the standard Galerkin approximation along with integration by parts, we obtain the following weak forms:

Step 1: Weak form of intermediate momentum

$$\int_\Omega \mathbf{N}_u^{\mathrm{T}}\Delta U_j^\star\,\mathrm{d}\Omega=\Delta t\left[-\int_\Omega \mathbf{N}_u^{\mathrm{T}}\frac{\partial}{\partial x_k}(u_kU_j)\,\mathrm{d}\Omega-\frac{1}{Re}\int_\Omega\frac{\partial\mathbf{N}_u^{\mathrm{T}}}{\partial x_i}(\tau_{ij}^n+\tau_{ij}^p)\,\mathrm{d}\Omega\right]^n$$
$$+\frac{(\Delta t)^2}{2}\left[\int_\Omega\frac{\partial}{\partial x_m}(u_m\mathbf{N}_u^{\mathrm{T}})\left(-\frac{\partial}{\partial x_k}(u_kU_j)+\frac{1}{Re}\frac{\partial\tau_{ij}^p}{\partial x_i}\right)\mathrm{d}\Omega\right]^n$$
$$+\Delta t\left[\int_\Gamma \mathbf{N}_u^{\mathrm{T}}\mathbf{t}_d\,\mathrm{d}\Gamma\right]^n \tag{15}$$

In the above equation $\mathbf{t}_d=[\tau_{ij}^n/Re]\mathbf{n}$ indicates the part of the traction corresponding to the stresses only and $\mathbf{n}$ are the components of the outward normal to the boundaries. As the pressure term is completely removed from the first step, we have only rest of the traction left in the equation.

Step 2: Weak form of pressure equation

$$\int_\Omega \mathbf{N}_p^{\mathrm{T}}\frac{1}{Re}\left(\frac{1}{\beta^2}\right)^n\Delta p\,\mathrm{d}\Omega=-\Delta t\int_\Omega\mathbf{N}_p^{\mathrm{T}}\frac{\partial}{\partial x_j}U_j^n\,\mathrm{d}\Omega$$
$$-\Delta t\int_\Gamma\mathbf{N}_p^{\mathrm{T}}\left(\Delta U_j^\star-\frac{\Delta t}{Re}\frac{\partial p^n}{\partial x_j}\right)n_j\,\mathrm{d}\Gamma$$
$$+\Delta t\int_\Omega\frac{\partial\mathbf{N}_p^{\mathrm{T}}}{\partial x_j}\left(\Delta U_j^\star-\frac{\Delta t}{Re}\frac{\partial p^n}{\partial x_j}\right)\mathrm{d}\Omega \tag{16}$$

In the above equation, pressure and ΔU_i^* terms are integrated by parts and n_j are the components of the outward normal to the boundaries.

DOI: 10.1002/fld

Step 3: Weak form of momentum correction

$$\int_\Omega \mathbf{N}_u^{\mathrm{T}} \Delta U_j \,\mathrm{d}\Omega = \int_\Omega \mathbf{N}_u^{\mathrm{T}} \Delta U_j^\star \,\mathrm{d}\Omega + \Delta t \int_\Omega \frac{\partial \mathbf{N}_u^{\mathrm{T}}}{\partial x_j} \frac{p^n}{Re} \,\mathrm{d}\Omega - \Delta t \int_\Gamma \mathbf{N}_u^{\mathrm{T}} \mathbf{t}_p \,\mathrm{d}\Gamma - \frac{(\Delta t)^2}{2Re} \left[\int_\Omega \frac{\partial}{\partial x_m} (u_m \mathbf{N}_u^{\mathrm{T}}) \frac{\partial p}{\partial x_j} \,\mathrm{d}\Omega \right]^n \tag{17}$$

In the above equation $\mathbf{t}_p = [(p^n + \theta_2 \Delta p)/Re]\mathbf{n}$ indicates only the part of the traction corresponding to the pressure that was removed from step 1. It is simply ignored and assumed to be zero as the full traction is prescribed in step 1 [39].

Step 4: Weak form of constitutive equation

$$\begin{aligned}
\int_\Omega \mathbf{N}_{\tau^p}^{\mathrm{T}} \Delta \tau_{ij}^p \,\mathrm{d}\Omega = \Delta t & \left[- \int_\Omega \mathbf{N}_{\tau^p}^{\mathrm{T}} \frac{\partial}{\partial x_k} (u_k \tau_{ij}^p) \,\mathrm{d}\Omega - \int_\Omega \mathbf{N}_{\tau^p}^{\mathrm{T}} \frac{\tau_{ij}^p}{De} \,\mathrm{d}\Omega \right]^n \\
& + \Delta t \left[\int_\Omega \mathbf{N}_{\tau^p}^{\mathrm{T}} \left(\tau_{ik}^p \frac{\partial u_j}{\partial x_k} + \tau_{jk}^p \frac{\partial u_i}{\partial x_k} \right) \mathrm{d}\Omega \right]^n \\
& + \Delta t \left[\frac{\alpha}{De} \int_\Omega \mathbf{N}_{\tau^p}^{\mathrm{T}} \left(\frac{\partial u_i}{\partial x_j} + \frac{\partial u_j}{\partial x_i} - \frac{2}{3} \frac{\partial u_k}{\partial u_k} \delta_{ij} \right) \mathrm{d}\Omega \right]^n \\
& + \frac{(\Delta t)^2}{2} \left[\int_\Omega \frac{\partial}{\partial x_m} (u_m \mathbf{N}_{\tau^p}^{\mathrm{T}}) \left(- \frac{\partial}{\partial x_k} (u_k \tau_{ij}^p) \right) \mathrm{d}\Omega \right]^n \\
& - \frac{(\Delta t)^2}{2} \left[\int_\Omega \frac{\partial}{\partial x_m} (u_m \mathbf{N}_{\tau^p}^{\mathrm{T}}) \frac{\alpha}{De} \left(\frac{\partial u_i}{\partial x_j} + \frac{\partial u_j}{\partial x_i} - \frac{2}{3} \frac{\partial u_k}{\partial u_k} \delta_{ij} \right) \mathrm{d}\Omega \right]^n \\
& - \frac{(\Delta t)^2}{2} \left[\int_\Omega \frac{\partial}{\partial x_m} (u_m \mathbf{N}_{\tau^p}^{\mathrm{T}}) \left(\tau_{ik}^p \frac{\partial u_j}{\partial x_k} + \tau_{jk}^p \frac{\partial u_i}{\partial x_k} \right) \mathrm{d}\Omega \right]^n \\
& - \frac{(\Delta t)^2}{2} \left[\int_\Omega \frac{\partial}{\partial x_m} (u_m \mathbf{N}_{\tau^p}^{\mathrm{T}}) \frac{\tau_{ij}^p}{De} \,\mathrm{d}\Omega \right]^n
\end{aligned} \tag{18}$$

The higher-order terms in the above equations act as convection stabilizing terms. The final matrix form of the four steps may be written as

Step 1: Intermediate momentum

$$\Delta \tilde{\mathbf{U}}^\star = -\mathbf{M}_u^{-1} \Delta t [(\mathbf{C}_u \tilde{\mathbf{U}} + \mathbf{K}_\tau \tilde{\mathbf{u}} + \mathbf{G}_{\tau^p} - \mathbf{f}_u) - \Delta t (\mathbf{K}_u \tilde{\mathbf{U}} + \mathbf{f}_s)]^n \tag{19}$$

Step 2: Pressure

$$(\mathbf{M}_p + \Delta t^2 \theta_1 \theta_2 \mathbf{H}) \Delta \tilde{\mathbf{p}} = \Delta t [\mathbf{G}_u \tilde{\mathbf{U}} + \theta_1 \mathbf{G}_u \Delta \tilde{\mathbf{U}}^\star - \Delta t \theta_1 \mathbf{H} \tilde{\mathbf{p}} - \mathbf{f}_p]^n \tag{20}$$

Step 3: Momentum correction

$$\Delta \tilde{\mathbf{U}} = \Delta \tilde{\mathbf{U}}^\star - \mathbf{M}_u^{-1} \Delta t [\mathbf{G}_p^{\mathrm{T}} (\tilde{\mathbf{p}}^n + \theta_2 \Delta \tilde{\mathbf{p}}) + \Delta t \mathbf{Q}_p \tilde{\mathbf{p}}^n] \tag{21}$$

DOI: 10.1002/fld

Step 4: Constitutive equation

$$\Delta\tilde{\boldsymbol{\tau}}^p = -\mathbf{M}_{\tau^p}^{-1}\Delta t[\mathbf{C}_{\tau^p}\tilde{\boldsymbol{\tau}}^p + \mathbf{K}_{\tau^p}\tilde{\boldsymbol{\tau}}^p - \mathbf{D}_{\tau^p}\tilde{\boldsymbol{\tau}}^p - \mathbf{D}_\tau]^n \tag{22}$$

where the velocity, pressure and extra stress variables are approximated using equal order interpolation functions at all computational points in the domain and the matrices are given as

$$\begin{aligned}
\mathbf{M}_u &= \int_\Omega \mathbf{N}_u^{\mathrm{T}}\mathbf{N}_u \,\mathrm{d}\Omega; \quad \mathbf{K}_\tau = \int_\Omega \mathbf{B}^{\mathrm{T}}\frac{(1-\alpha)}{Re}\left(\mathbf{I}_o - \frac{2}{3}\mathbf{m}\mathbf{m}^{\mathrm{T}}\right)\mathbf{B}\,\mathrm{d}\Omega \\
\mathbf{C}_u &= \int_\Omega \mathbf{N}_u^{\mathrm{T}}(\boldsymbol{\nabla}^{\mathrm{T}}(\mathbf{u}\mathbf{N}_u))\,\mathrm{d}\Omega; \quad \mathbf{G}_{\tau^p} = \int_\Omega \frac{1}{Re}\mathbf{N}_u^{\mathrm{T}}(\boldsymbol{\nabla}^{\mathrm{T}}(\boldsymbol{\tau}^p N_{\tau^p}^*))\,\mathrm{d}\Omega \\
\mathbf{K}_u &= -\frac{1}{2}\int_\Omega (\boldsymbol{\nabla}^{\mathrm{T}}(\mathbf{u}\mathbf{N}_u))^{\mathrm{T}}(\boldsymbol{\nabla}^{\mathrm{T}}(\mathbf{u}\mathbf{N}_u))\,\mathrm{d}\Omega; \quad \mathbf{f}_u = \int_\Gamma \mathbf{N}_u^{\mathrm{T}}\mathbf{t}_d\,\mathrm{d}\Gamma \\
\mathbf{M}_p &= \int_\Omega \mathbf{N}_p^{\mathrm{T}}\left(\frac{1}{Re\beta^2}\right)^n \mathbf{N}_p\,\mathrm{d}\Omega; \quad \mathbf{H} = \int_\Omega \frac{1}{Re}(\boldsymbol{\nabla}\mathbf{N}_p)^{\mathrm{T}}\boldsymbol{\nabla}\mathbf{N}_p\,\mathrm{d}\Omega \\
\mathbf{f}_p &= \Delta t\int_\Gamma \mathbf{N}_p^{\mathrm{T}}\left[\mathbf{N}_u\tilde{\mathbf{U}}^n + \theta_1\left(\Delta\tilde{\mathbf{U}}^\star - \frac{\Delta t}{Re}\boldsymbol{\nabla}p^{n+\theta_2}\right)\right]\mathbf{n}^{\mathrm{T}}\,\mathrm{d}\Gamma \\
\mathbf{G}_p &= \int_\Omega \frac{1}{Re}(\boldsymbol{\nabla}\mathbf{N}_p)^{\mathrm{T}}\mathbf{N}_u\,\mathrm{d}\Omega; \quad \mathbf{C}_{\tau^p} = \int_\Omega \mathbf{N}_{\tau^p}^{\mathrm{T}}(\boldsymbol{\nabla}^{\mathrm{T}}(\mathbf{u}\mathbf{N}_{\tau^p}))\,\mathrm{d}\Omega \\
\mathbf{M}_{\tau^p} &= \int_\Omega \mathbf{N}_{\tau^p}^{\mathrm{T}}\mathbf{N}_{\tau^p}\,\mathrm{d}\Omega; \quad \mathbf{K}_{\tau^p} = \frac{\mathbf{M}_{\tau^p}}{De} \\
\mathbf{D}_\tau &= \int_\Omega \frac{\alpha}{De}\mathbf{N}_{\tau^p}^{\mathrm{T}}(\boldsymbol{\nabla}^{\mathrm{T}}(\mathbf{u}\mathbf{N}_u))\,\mathrm{d}\Omega; \quad \mathbf{G}_u = \int_\Omega (\boldsymbol{\nabla}\mathbf{N}_p)^{\mathrm{T}}\mathbf{N}_u\,\mathrm{d}\Omega \\
\mathbf{D}_{\tau^p} &= \int_\Omega \mathbf{N}_{\tau^p}^{\mathrm{T}}(\boldsymbol{\nabla}^{\mathrm{T}}(\mathbf{u}\mathbf{N}_u))\,\mathrm{d}\Omega; \quad \mathbf{Q}_p = \frac{1}{2Re}\int_\Omega (\boldsymbol{\nabla}^{\mathrm{T}}(\mathbf{u}\mathbf{N}_u))^{\mathrm{T}}\boldsymbol{\nabla}\mathbf{N}_p\,\mathrm{d}\Omega \\
\mathbf{f}_s &= \frac{1}{2}\int_\Omega (\boldsymbol{\nabla}^{\mathrm{T}}(\mathbf{u}\mathbf{N}_u))^{\mathrm{T}}(\boldsymbol{\nabla}^{\mathrm{T}}(\boldsymbol{\tau}^p\mathbf{N}_{\tau^p}))\,\mathrm{d}\Omega
\end{aligned} \tag{23}$$

In the above equation, the strain shape function matrix $\mathbf{B}$ is given as

$$\mathbf{B} = \mathbf{S}\mathbf{N}_u \tag{24}$$

where $\mathbf{S}$ is a strain matrix operator derived from the deviatoric stress and strain relations. For a two-dimensional case, it can be written as

$$\mathbf{S} = \begin{Bmatrix} \dfrac{\partial}{\partial x_1} & 0 \\ 0 & \dfrac{\partial}{\partial x_2} \\ \dfrac{\partial}{\partial x_2} & \dfrac{\partial}{\partial x_1} \end{Bmatrix} \tag{25}$$

$$\mathbf{m} = [1, 1, 0]^{\mathrm{T}} \tag{26}$$

DOI: 10.1002/fld

and

$$\mathbf{I}_o = \begin{bmatrix} 2 & & \\ & 2 & \\ & & 1 \end{bmatrix} \tag{27}$$

3. DOMAIN, BOUNDARY CONDITIONS AND STEADY-STATE CONVERGENCE

3.1. Computational domain

The computational domain consists of a stationary circular cylinder placed in a rectangular channel at a distance of $12R$ from the inlet, where R is the radius of the cylinder. The distance from the centre of the cylinder to the channel walls is equal to $2R$. The total distance from inlet to exit section is $28R$. The geometry and boundary conditions are shown in Figure 1.

A total of four unstructured meshes were generated. They were generated by changing the degree of refinement close to the region around the cylinder. Figure 2 shows the four meshes in the vicinity of the cylinder. The typical element size on the cylinder wall for the four meshes used are, respectively, 0.10924, 0.05474, 0.00633 and 0.00137.

As mentioned before, the Oldroyd-B model is employed in the present study and a viscosity rate of $\alpha = 0.41$ is assumed. The convection terms in the momentum equations are assumed to be zero to obtain equations for creeping viscoelastic flows.

3.2. Boundary conditions

The inlet and exit velocity profiles are assumed to be fully developed and they are given as

$$u_1 = 1.5\left(1 - \frac{x_2^2}{4}\right) \tag{28}$$

$$u_2 = 0 \tag{29}$$

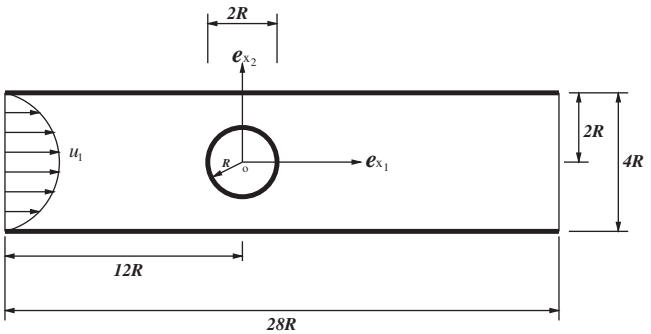

Figure 1. Viscoelastic flow past a circular cylinder placed in a rectangular channel.

DOI: 10.1002/fld

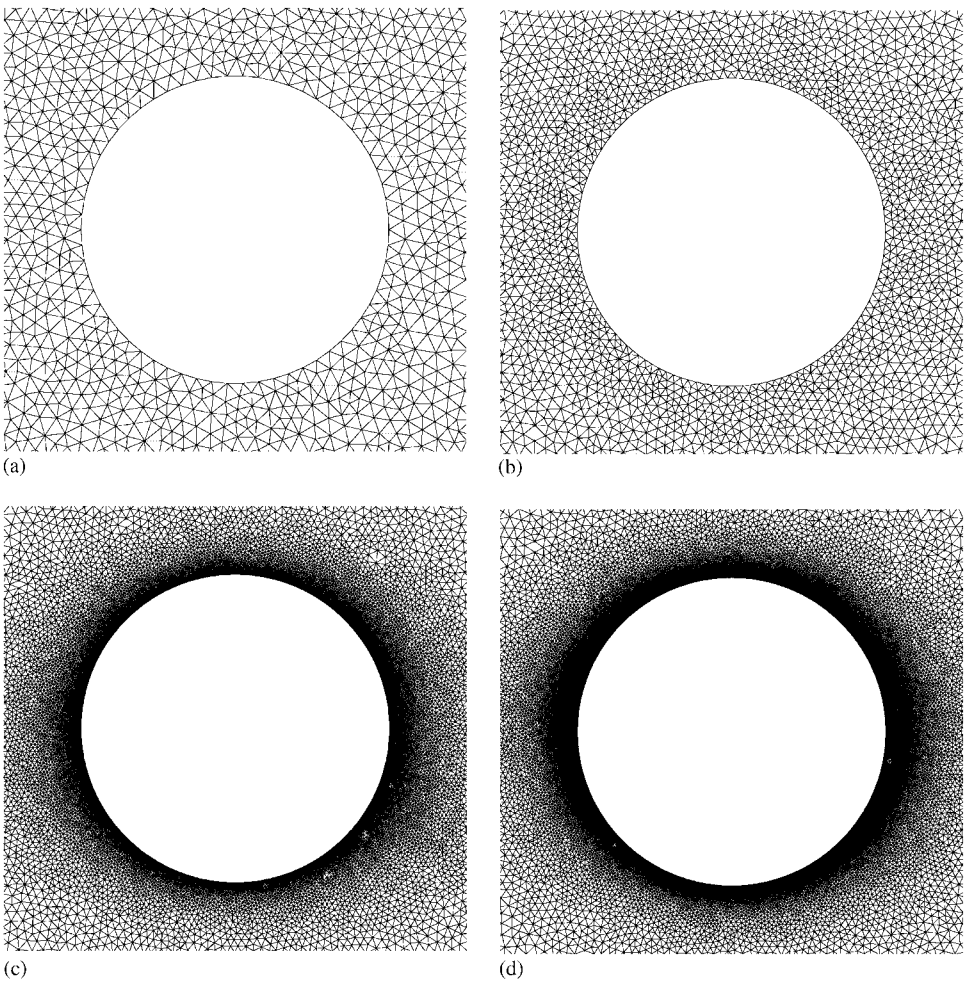

Figure 2. Oldroyd-B fluid flow past a circular cylinder: (a) mesh A (nodes: 13 977; elements: 27 267; $\Delta d = 0.10924$); (b) mesh B (nodes: 16 690; elements: 32 617; $\Delta d = 0.05474$); (c) mesh C (nodes: 33 189; elements: 64 759; $\Delta d = 0.00633$); and (d) mesh D (nodes: 82 856; elements: 160 978; $\Delta d = 0.00137$).

On the channel solid walls and cylinder surface, no slip conditions are assumed. On the basis of the fully developed hypothesis, the steady distributions of extra stresses at the inlet section in their non-dimensional form are given as [44]

$$\tau_{11}^p = 2\alpha De \left(\frac{\partial u_1}{\partial x_2} \right)^2 \tag{30}$$

$$\tau_{12}^p = \alpha \frac{\partial u_1}{\partial x_2} \tag{31}$$

$$\tau_{22}^p = 0 \tag{32}$$

DOI: 10.1002/fld

The extra stresses on the channel walls are identical to inlet section (Equations (30)–(32)) [11, 20]. After several numerical calculations by employing different boundary conditions on the cylinder wall, we found that prescribing no boundary conditions for the extra stresses on the cylinder wall gives the best solution. Therefore, no extra stress boundary conditions are prescribed on the cylinder wall in the present study.

3.3. Steady-state convergence

The steady-state convergence criterion is fixed based on the L_2 norm of the residual of the equations. Here, the norm of difference between time step $n+1$ and n quantities is normalized by the quantities at time step $n+1$. It is given as

$$\|e\|_2^{\phi} = \frac{[\sum_{i=1}^{m}(\|\boldsymbol{\phi}\|_i^{n+1} - \|\boldsymbol{\phi}\|_i^{n})^2]^{1/2}}{[\sum_{i=1}^{m}(\|\boldsymbol{\phi}\|_i^{n+1})^2]^{1/2}} \tag{33}$$

where m is the number of nodes, ϕ indicates the extra stress components and velocity. The above tolerance was reduced to a value of at least 10^{-6} for extra stresses and 10^{-8} for velocity components to assume a steady state.

4. POSITIVE DEFINITIVENESS AND ARTIFICIAL DAMPING

The performance of computational methods for creeping viscoelastic flows is often monitored by calculating the eigenvalues of an additional stress tensor [45]. In this study, we also monitored the additional stress tensor, which is referred to as the conformation tensor and is defined as $\tau_{ij} = \tau_{ij}^{p} + (\alpha/De)\delta_{ij}$. It is anticipated that the additional stress tensor remains positive definite at lower Deborah numbers. At higher Deborah numbers, positive definitiveness may be lost without additional damping introduced to the discrete constitutive equations. As far as we are aware, there are only two papers on Oldroyd-B fluid flow past a circular cylinder to explicitly monitor the positive definiteness of the conformation tensor, although some works construct methods to preserve positive definitiveness [18]. Caola *et al.* [16] produced results up to a Deborah number of unity without losing the positive definiteness of the conformation tensor. However, their method failed to give steady-state solution beyond a Deborah number of unity. There are two important differences between the present and Caola *et al.*'s results. They used structured mesh and their steady-state convergence criterion is less stringent than the present results. However, their finest mesh consists of slightly smaller element size than the mesh we employed in the calculations. Another structured mesh-based methodology presented by Coronado *et al.* [15] predicted results without losing the positive definitiveness of the conformation matrix up to a Deborah number of 0.7.

The obvious step for preserving the positive definitiveness in the present explicit method is to add artificial damping to the discrete constitutive equations at the fourth step of the CBS scheme. In this study, we introduce one such way of improving the solution *via* an additional artificial damping [20]. Such an artificial damping can also eliminate the negative eigenvalues of the conformation matrix from the flow field. We briefly explain the theory behind the method below.

The artificial damping used here is an approximate second derivative-based method [20, 40, 46] and it can be added to the discrete constitutive equations if necessary. Although the method has been employed widely in the aerospace applications, this is relatively new to the viscoelastic flows.

DOI: 10.1002/fld

For completeness, the method is presented here. The following pressure switch-based artificial damping is added to the discrete form of the constitutive equation (22)

$$\Delta t \mathbf{M}_{\tau^p}^{-1} \frac{C_e S_e}{\Delta t} (\mathbf{M}_{\tau^p} - \mathbf{M}_{\tau^p L}) \underline{\tilde{\boldsymbol{\tau}}}^p \tag{34}$$

where $\mathbf{M}$ is the mass matrix and subscript L indicates a lumped matrix. The difference between the consistent and lumped mass matrix along with the nodal extra stress values obtained in the above equation is a result of the approximation used to calculate second-order derivatives of extra stresses. S_e in the above equation is an elementally averaged nodal pressure switch calculated on the nodes as

$$S_i = \frac{|\sum_1^n (p_i - p_k)|}{\sum_1^n |p_i - p_k|} \tag{35}$$

where n is the number of nodes connected to i. In Equation (34) C_e is an user specified constant. This value should be as small as possible to minimize the adverse influence of the extra dissipation. As mentioned previously, Equation (34) is derived from approximation of second derivatives of the extra stresses. However, the method can also be used without this approximation as explained in Reference [40] but this needs slightly more computational time to calculate second derivatives. The pressure switch (Equation (35)) can also be replaced with another similar switch constructed from extra stress or other variables if necessary.

5. RESULTS AND DISCUSSIONS

Both quantitative and qualitative results are presented in this section. The drag force per unit length of the circular cylinder is the major quantity used in the discussions and it is calculated in non-dimensional form as

$$D = \int_0^{2\pi} [(-p + \tau_{11}^n + \tau_{11}^p)\cos\theta + (\tau_{12}^n + \tau_{12}^p)\sin\theta] R \, \mathrm{d}\theta \tag{36}$$

The mesh convergence histories of drag force with respect to mesh size, for a Deborah number range between 0.0 and 3.0, are given in Figures 3 and 4. In Figure 3, convergence histories for some selected Deborah numbers are given and compared against convergence histories provided by other researchers. These convergence histories are obtained without adding any additional damping. Convergence histories for all Deborah numbers considered in the present study are shown in Figure 4. These figures show that, overall, the drag force converges reasonably on the unstructured meshes used. At lower Deborah numbers, the drag forces obtained move towards zero element size results given by Dou *et al.* [11]. The convergence history shows an increase in drag force value with a decrease in element size up to a Deborah number value of 0.4. Beyond this value the opposite trend is noticed. Figure 3 shows the convergence histories for Deborah numbers 0.3, 0.5, 0.7 and higher values. The present convergence history is also compared against the convergence history given by Dou and Phan-Thien [11]. It is important to note here that the value given by Dou and Phan-Thien, at zero mesh size, is an extrapolated value from their numerical study. Their original study was only carried out on relatively coarse meshes. As seen, the present drag force value at $De = 0.3$ is very close to the value predicted by Dou and Phan-Thien. It is also noted that at all other Deborah number values, present results are lower than the ones given in the literature.

DOI: 10.1002/fld

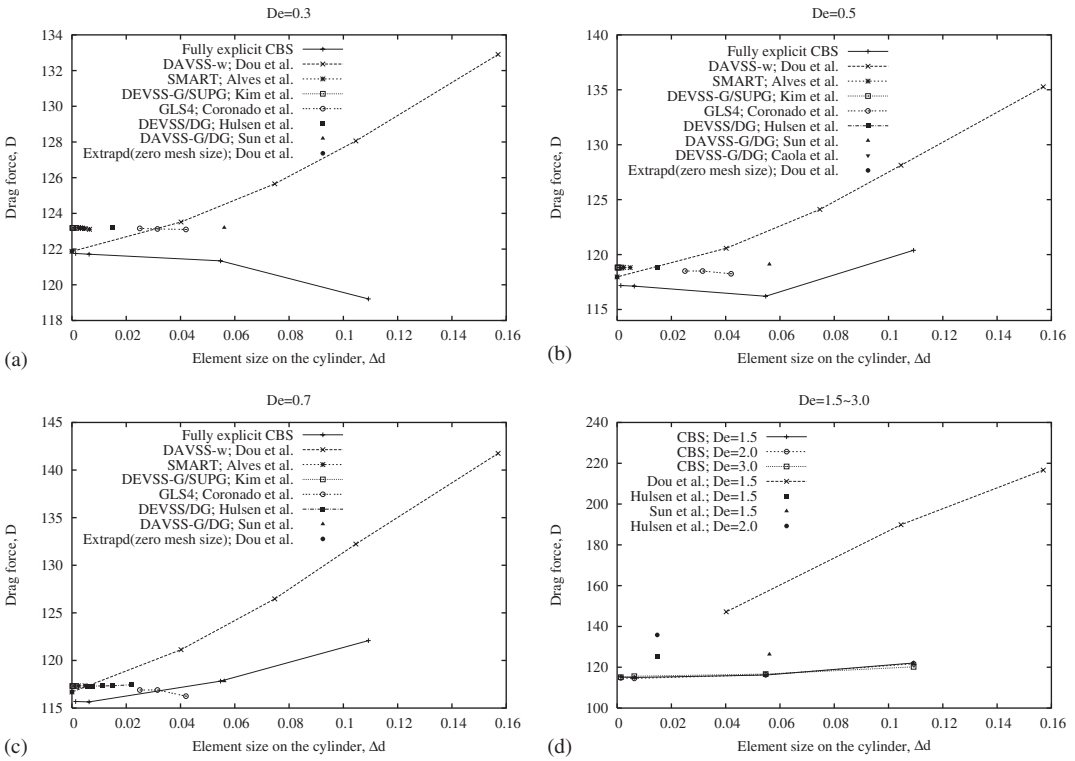

Figure 3. Oldroyd-B fluid flow past a circular cylinder. Comparison of drag force distribution against typical element size on the cylinder surface for different Deborah numbers: (a) $De=0.3$; (b) $De=0.5$; (c) $De=0.7$; and (d) $De=1.5$–3.0.

For $De=0.5$ and 0.7, present drag force values are slightly lower than Dou and Phan-Thien but very close to the zero mesh value predicted by Dou and Phan-Thien. This trend continues for the higher Deborah numbers, as shown in Figures 3 and 4. Unlike Dou and Phan-Thien's results, the change in the drag force in the present study with refinement is small. This indicates that even on coarse meshes the solution obtained here is close to the expected, converged solution. In other words, CBS solution presented in this study shows a faster convergence. As mentioned in the Introduction, many schemes failed to give a steady-state solution at Deborah numbers 0.7 and above, especially on very fine meshes. However, the CBS procedure presented is converged to a steady-state solution, even on the finest mesh used. At a Deborah number of 0.7, the CBS method gives a solution close to Sun *et al.* [10] and Coronado *et al.* [15] at around the element sizes of 0.0561 and 0.0315 as shown in Figure 3(c). However, the present value of drag force is further reduced with decrease in element size. Figure 3 also shows the mesh convergence histories for Deborah numbers between 1.5 and 3.0. The drag values are compared against published results wherever possible. It appears that the convergence is good.

Although, the percentage of difference between the present and other reported results is small, the expected upward trend in the drag force beyond a Deborah number value of approximately 0.7 is not observed. The downward trend of the predicted drag force may be the result of lack of

DOI: 10.1002/fld

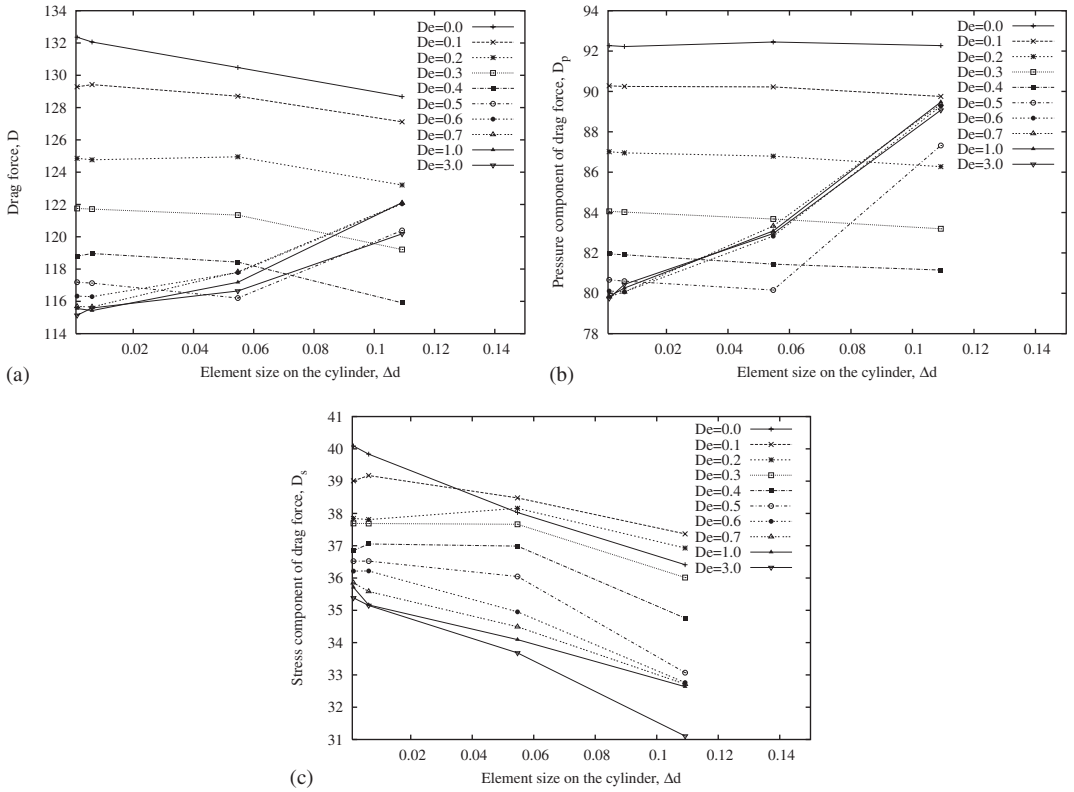

Figure 4. Oldroyd-B fluid flow past a circular cylinder. Comparison of the (a) total drag force, (b) pressure part of the drag force and (c) stress part of the drag force distribution against typical element size on the cylinder surface for different Deborah numbers.

dissipation and may also be a result of conformation matrix losing positive definitiveness. However, one of best solutions available for viscoelastic flow past a circular cylinder [16] is not far from the results given by the present CBS method. Caola *et al.*'s [16] results show no sudden increase in drag force beyond a Deborah number of 0.7. However, many other studies predict a rapid increase in drag force beyond a Deborah number of 0.7. In the following paragraphs, we attempt to find more explanation on the behaviour of the CBS method and its accuracy. It is also clear from Figure 4 that the mesh convergence is reasonable over the range of Deborah numbers considered without the addition of any artificial damping.

Since the drag force predicted was not showing the expected trend, we monitored the eigenvalues of the conformation tensor. It was clear from the results that the conformation tensor was losing positive definitiveness beyond a Deborah number of 0.7. However, by switching the artificial damping on and by adding sufficient damping just enough to remove negative eigenvalues, we are able to retain positive definitiveness of the conformation tensor. So far, we are able to obtain solutions up to a Deborah number of 2 without losing positive definitiveness.

Figure 5(a) shows comparison of the total drag force at different Deborah numbers obtained from all the four meshes without the addition of the artificial damping. The solutions were also

DOI: 10.1002/fld

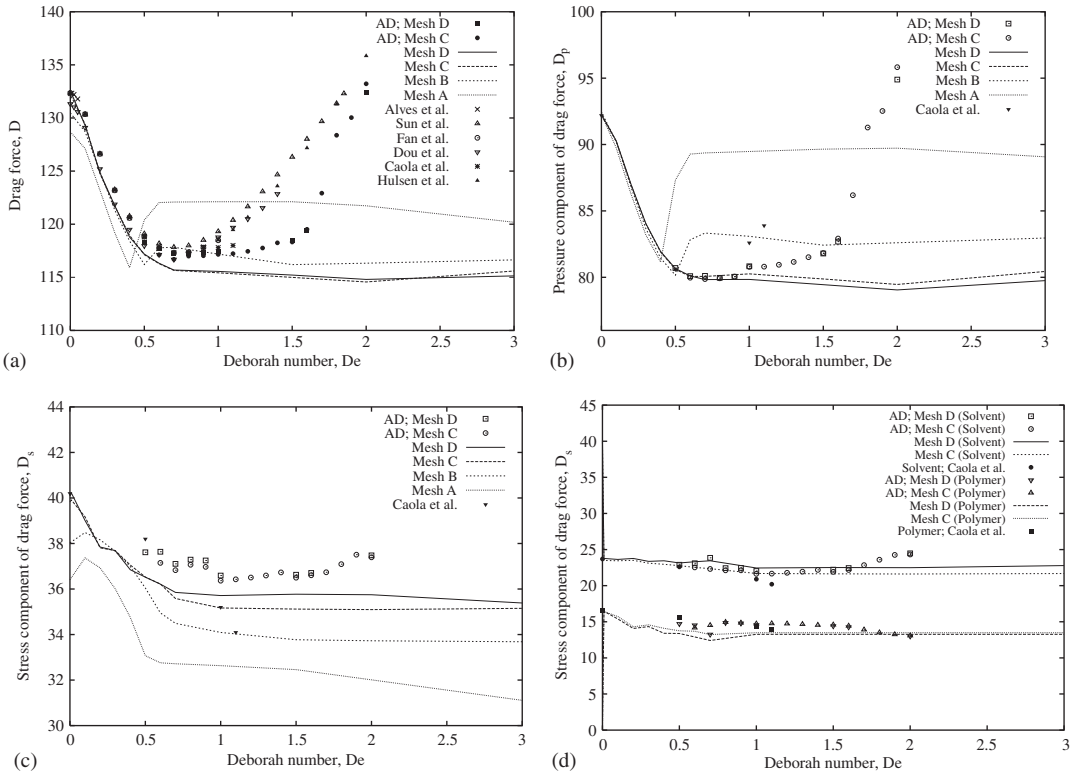

Figure 5. Oldroyd-B fluid flow past a circular cylinder. Drag force distribution on different unstructured meshes used: (a) total drag; (b) pressure; (c) total stress; and (d) Newtonian/non-Newtonian stress.

obtained with the artificial damping on meshes C and D. As seen, the results obtained from Mesh A (without damping) is not only away from other numerical results but also has a sudden jump in the drag force value close to a Deborah number of 0.4. This is also evident from the pressure component of the drag force shown in Figure 5(b). Further refinement increases the accuracy, but the jump in the drag force and pressure is still visible on Mesh B (without damping), although delayed to a Deborah number value of around 0.5. Meshes C and D, (without damping) on the other hand, have given a smoother drag force and pressure distributions. Between the meshes C and D, (without damping) the difference in total drag force is very small, demonstrating that the drag force is converged to a stable value. However, the pressure distribution paints a different picture. As seen from Figure 5(b) the pressure convergence is excellent up to a Deborah number value of about unity. Beyond this limit, the pressure value predicted by the meshes C and D shows the signs of minor divergence. The trend given by the stress component in Figure 5(c) is consistent with the observation that the stress component values are converged up to a Deborah number value of 0.7. Beyond this value, although the meshes C and D give smooth stress field, the convergence is not satisfactory. Figure 5(d) shows the distribution of solvent and polymer contribution of the drag forces.

DOI: 10.1002/fld

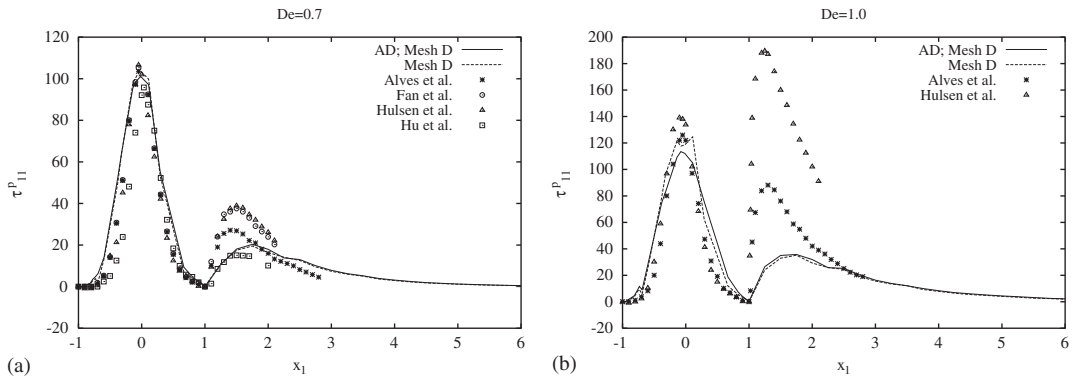

Figure 6. Oldroyd-B fluid flow past a circular cylinder. Distribution of τ_{11} along cylinder surface and in the wake: (a) $De = 0.7$ and (b) $De = 1.0$.

As seen the agreement of total drag force between the present and other results is excellent up to a Deborah number of 0.7 without the addition of any additional damping. Beyond this value, even the trend is not quite the same as in the majority of other numerical results. However, when the negative eigenvalues are eliminated by adding the extra artificial damping, the drag force obtained is quite close to Caola *et al.* [16] (see Figure 5(a)). It is also noticed that the upward trend in drag force beyond a Deborah number of 0.7 is obtained when the additional damping is added. This clearly shows that the additional damping is important in increasing the accuracy of computation. In addition to obtaining a result very close to the fine mesh result presented by Caola *et al.* [16], the artificial damping has also helped in obtaining the expected trend in drag force variation.

As mentioned before, some of the earlier works on flow past cylinder have blamed a steep increase in extra stress value close to the rear and front stagnation points for the solution breakdown. To assess the influence of the extra stress values close to the stagnation points, the extra stress component τ^p_{11} is plotted in Figure 6 along the domain centreline. From the figures, it is clear that large peak values of the stresses are predicted on the cylinder surface. However, the peak extra stress values and their gradients predicted by CBS scheme at the rear stagnation point are substantially lower than the values predicted by others. This may be another reason why CBS scheme gives steady-state solution for Oldroyd-B fluid for higher Deborah numbers. Even with the addition of the artificial damping, the stagnation value of extra stresses is not changed dramatically.

To further explain the use of artificial damping, the eigenvalues with and without the inclusion of artificial damping are compared in Figure 7 for a Deborah number of 0.7. The figures on the left show the eigenvalue contours without the additional dissipation and the ones on the right show the contours with the dissipation switched on. A C_e value of 5×10^{-4} was used in Equation (34) to switch on the additional dissipation. As seen in Figure 7, the additional dissipation has eliminated negative eigenvalues and it also has reduced spatial oscillations. The additional dissipation has also contributed to a small increase in the total drag value. The total drag force calculated is 116.696, when the additional dissipation is switched on as compared with 115.651 without dissipation.

In Table I, comparison between the CBS results with and without damping and several other numerical experiments are presented. The drag forces are in an excellent agreement with the

DOI: 10.1002/fld

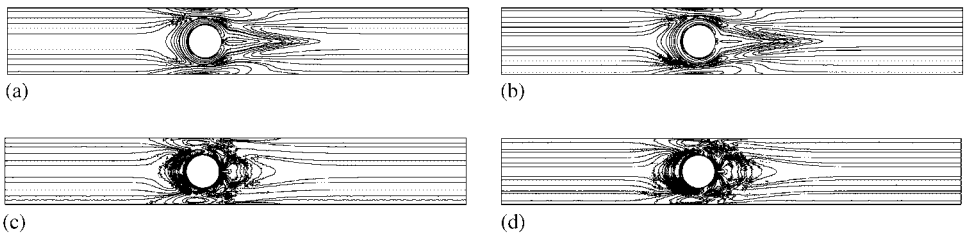

Figure 7. Eigenvalues of additional stress tensor $\tau_{ij}=\tau_{ij}^{p}+(\alpha/De)\delta_{ij}$ for Oldroyd-B fluid flow past a circular cylinder. Without(left)/with(right) artificial dissipation at $De=0.7$: (a) λ_1 contours: $\lambda_{1_{\min}}=0.58$, $\lambda_{1_{\max}}=111.06$; (b) λ_1 contours: $\lambda_{1_{\min}}=0.58$, $\lambda_{1_{\max}}=107.07$; (c) λ_2 contours: $\lambda_{2_{\min}}=0.0$, $\lambda_{2_{\max}}=0.70$; and (d) λ_2 contours: $\lambda_{2_{\min}}=-0.03$, $\lambda_{2_{\max}}=0.76$.

Table I. Drag force calculations by using CBS scheme with the Oldroyd-B model.

	Mesh D		Mesh C		The other availably numerical results					
De	CBS	CBS AD	CBS	CBS AD	[16]	[10]	[11]	[18]	[14]	[17]
0.0	132.357		132.060		132.30	132.34	131.32	132.358	132.36	
0.01	132.245		131.917							
0.1	129.288		129.422			130.33	129.09	130.363	130.36	130.343
0.2	124.856		124.766			126.63	125.20	126.626	126.62	126.618
0.3	121.753		121.714			123.26	121.87	123.193	123.19	123.195
0.4	118.798		118.962			120.76	119.50	120.596	120.59	120.596
0.5	117.185	118.314	117.127		118.80	119.11	117.97	118.836	118.83	118.832
0.6	116.324	117.728	116.290	117.121		118.17	117.13	117.792	117.77	117.786
0.7	115.684	117.214	115.651	116.696		117.84	116.69	117.340	117.32	117.328
0.8		117.252		116.994		117.98	117.23	117.373	117.36	117.370
0.9		117.291		117.030		118.50	117.89	117.787	117.79	117.865
1.0	115.556	117.418	115.427	117.154	117.80	119.32	118.78	118.501	118.49	118.560
1.1				117.230	118.00	120.39	119.69	119.466		
1.2				117.450		121.65	120.50	120.650		
1.3				117.757		123.07	121.54			
1.4				118.248		124.66	122.86	123.587		
1.5	115.215	118.422	114.992	118.321		126.32				
1.6		119.393		119.522		128.01		127.172		
1.7				122.921		129.67				
1.8				128.373		131.37		131.285		
1.85						132.30				
1.9				130.035						
2.0	114.801	132.372	114.561	133.216				135.839		
3.0	115.137		115.592							

available data at lower Deborah numbers with and without damping. Although drag values, without damping decrease beyond a Deborah number of 0.7, the trend is reversed when the negative eigenvalues are eliminated using the artificial damping. Among the results compared in Table I, Caola *et al.*'s [16] fine mesh solution agrees more closely with the present results. However, at Deborah numbers beyond 1.7 present results are in good agreement with majority of the reported results.

DOI: 10.1002/fld

6. CONCLUSIONS

This research was targeted at using the CBS scheme to solve viscoelastic flow over a stationary circular cylinder placed in a rectangular channel. The Oldroyd-B model was used in this paper. One of the major problems of Oldrod-B model is the convergence to steady state beyond a Deborah number of unity. In this paper we have demonstrated that the CBS scheme gives steady-state results up to a Deborah number of three with a potential to enhance this limit further. We used an artificial damping scheme to retain positive definitiveness of the conformation tensor. We demonstrated that adding an additional damping increases the drag value and also makes the negative eigenvalues of the conformation tensor disappear, in addition to giving a smoother and more accurate solution. The major conclusions derived from the present study are:

- The CBS scheme is capable of numerically predicting Oldroyd-B fluid flow up to a Deborah number of 3. It is clear that most of the models agree excellently up to a Deborah number value of 0.7.
- The mesh convergence studies carried out clearly indicate that the convergence is reasonable at all Deborah numbers considered.
- At higher Deborah numbers, the agreement with other numerical solution is poor when no artificial damping was added. It is also obvious from the fine mesh solution of Caola *et al.* [16] that drag force does not necessarily increase as dramatically as predicted by some previous works. Caola *et al.*'s results closely agree with the present predictions than the other numerical results.
- We demonstrated that artificial damping is needed to eliminate the negative eigenvalues of the conformation matrix. This resulted in the expected trend in drag force variation. A careful tuning of the artificial damping constant is needed to obtain an optimal artificial damping.
- Further investigation on using a variety of viscoelastic flow models, such as upper convected Maxwell (UCM) and Phan-Thien/Tanner (PTT) models, may further increase the understanding and behaviour of the CBS scheme.

ACKNOWLEDGEMENTS

This research is funded by the Engineering and Physical Sciences Research Council (EPSRC) grant no. EP/C515498/1.

REFERENCES

1. Baaijens FPT. Mixed finite element methods for viscoelastic flows: a review. *Journal of Non-Newtonian Fluid Mechanics* 1998; **79**:361–385.
2. Perera MGN, Walters K. Long-range memory effects in flows involving abrupt changes in geometry: Part I: flows associated with I-shaped and T-shaped geometries. *Journal of Non-Newtonian Fluid Mechanics* 1977; **2**:49–81.
3. Rajagopalan D, Armstrong RC, Brown RA. Finite element methods for calculation of steady, viscoelastic flow using constitutive equations with a Newtonian viscosity. *Journal of Non-Newtonian Fluid Mechanics* 1990; **36**:159–192.
4. King RC, Apelian MR, Armstrong RC, Brown RA. Numerically stable finite element techniques for viscoelastic calculations in smooth and singular geometries. *Journal of Non-Newtonian Fluid Mechanics* 1988; **29**:147–216.
5. Rajagopalan D, Armstrong RC, Brown RA. Calculation of steady viscoelastic flow using a multimode Maxwell model: application of the explicitly elliptic momentum equation (EEME) formulation. *Journal of Non-Newtonian Fluid Mechanics* 1990; **36**:135–157.

DOI: 10.1002/fld

6. Brown RA, Szady MJ, Northey PJ, Armstrong RC. On the numerical stability of mixed finite-element methods for viscoelastic flows governed by differential constitutive equations. *Theoretical and Computational Fluid Dynamics* 1993; **5**:77–106.
7. Sun J, Phan-Thien N, Tanner RI. An adaptive viscoelastic stress splitting scheme and its applications: AVSS/SI and AVSS/SUPG. *Journal of Non-Newtonian Fluid Mechanics* 1996; **65**:75–91.
8. Guénette R, Fortin M. A new mixed finite element method for computing viscoelastic flows. *Journal of Non-Newtonian Fluid Mechanics* 1995; **60**:27–52.
9. Liu AW, Bornside DE, Armstrong RC, Brown RA. Viscoelastic flow of polymer solutions around a periodic, linear array of cylinders: comparisons of predictions for microstructure and flow fields. *Journal of Non-Newtonian Fluid Mechanics* 1998; **77**:153–190.
10. Sun J, Smith MD, Armstrong RC, Brown RA. Finite element method for viscoelastic flows based on the discrete adaptive viscoelastic stress splitting and the discontinuous Galerkin method: DAVSS-G/DG. *Journal of Non-Newtonian Fluid Mechanics* 1999; **86**:281–307.
11. Dou HS, Phan-Thien N. The flow of an Oldroyd-B fluid past a cylinder in a channel: adaptive viscosity vorticity (DAVSS-ω) formulation. *Journal of Non-Newtonian Fluid Mechanics* 1999; **87**:47–73.
12. Phan-Thien N, Dou HS. Viscoelastic flow past a cylinder: drag coefficient. *Computer Methods in Applied Mechanics and Engineering* 1999; **180**:243–266.
13. Dou HS, Phan-Thien N. Parallelisation of an unstructured finite volume code with PVM: viscoelastic flow around a cylinder. *Journal of Non-Newtonian Fluid Mechanics* 1998; **77**:21–51.
14. Fan Y, Tanner RI, Phan-Thien N. Galerkin/least-square finite-element methods for steady viscoelastic flows. *Journal of Non-Newtonian Fluid Mechanics* 1999; **84**:233–256.
15. Coronado OM, Arora D, Behr M, Pasquali M. Four-field Galerkin/least-squares formulation for viscoelastic fluids. *Journal of Non-Newtonian Fluid Mechanics* 2006; **140**:132–144.
16. Caola AE, Joo YL, Armstrong RC, Brown RA. Highly parallel time integration of viscoelastic flows. *Journal of Non-Newtonian Fluid Mechanics* 2001; **100**:191–216.
17. Alves MA, Pinho FT, Oliveira PJ. The flow of viscoelastic fluids past a cylinder: finite-volume high-resolution methods. *Journal of Non-Newtonian Fluid Mechanics* 2001; **97**:207–232.
18. Hulsen MA, Fattal R, Kupferman R. Flow of viscoelastic fluids past a cylinder at high Weissenberg number: stabilized simulations using matrix logarithms. *Journal of Non-Newtonian Fluid Mechanics* 2005; **127**:27–39.
19. Kim JM, Kim C, Ahn KH, Lee SJ. An efficient iterative solver and high-resolution computations of the Oldroyd-B fluid flow past a confined cylinder. *Journal of Non-Newtonian Fluid Mechanics* 2004; **123**:161–173.
20. Nithiarasu P. A fully explicit characteristic based split (CBS) scheme for viscoelastic flow calculations. *International Journal for Numerical Methods in Engineering* 2004; **60**:949–978.
21. Chorin AJ. Numerical solution of Navier–Stokes equations. *Mathematics of Computation* 1968; **22**:745–762.
22. Strikwerda JC, Lee YS. The accuracy of the fractional step method. *SIAM Journal on Numerical Analysis* 1999; **37**:37–47.
23. Brown D, Cortez R, Minion M. Accurate projection methods for the incompressible Navier–Stokes equations. *Journal of Computational Physics* 2001; **168**:464.
24. Chang W, Giraldo F, Perot B. Analysis of an exact fractional step method. *Journal of Computational Physics* 2002; **18**:183–199.
25. Nithiarasu P, Zienkiewicz OC. Analysis of an explicit and matrix free fractional step method for incompressible flows. *Computer Methods in Applied Mechanics and Engineering* 2006; **195**:5537–5551.
26. Codina R. Pressure stability in fractional step finite element methods for incompressible flows. *Journal of Computational Physics* 2001; **170**:112–140.
27. Lóhner R, Morgan K, Zienkiewicz OC. The solution of non-linear hyperbolic equation systems by the finite element method. *International Journal for Numerical Methods in Fluids* 1984; **4**:1043–1063.
28. Nithiarasu P, Codina R, Zienkiewicz OC. The characteristic based split (CBS) scheme—a unified approach to fluid dynamics. *International Journal for Numerical Methods in Engineering* 2006; **66**:1514–1546.
29. Zienkiewicz OC, Codina R. A general algorithm for compressible and incompressible flow—part I. the split, characteristic-based scheme. *International Journal for Numerical Methods in Fluids* 1995; **20**:869–885.
30. Zienkiewicz OC, Nithiarasu P. A universal algorithm for fluid dynamics. The characteristic based split (CBS) procedure. Some tests on stability and boundary conditions. *Archives of Mechanics* 2000; **52**:857–887.
31. Massarotti N, Nithiarasu P, Zienkiewicz OC. Characteristic-based-split (CBS) algorithm for incompressible flow problems with heat transfer. *International Journal of Numerical Methods for Heat and Fluid Flow* 2001; **8**:969–990.

DOI: 10.1002/fld

32. Nithiarasu P, Mathur JS, Weatherill NP, Morgan K. Three dimensional incompressible flow calculations using the characteristic based split (CBS) scheme. *International Journal for Numerical Methods in Fluids* 2004; **44**:1207–1229.
33. Nithiarasu P, Liu CB. An artificial compressibility based characteristic based split (CBS) scheme for steady and unsteady turbulent incompressible flows. *Computer Methods in Applied Mechanics and Engineering* 2006; **195**:2961–2982.
34. Zienkiewicz OC, Satya Sai BVK, Morgan K, Codina R, Vázquez M. A general algorithm for compressible and incompressible flow—part II. Tests on the explicit form. *International Journal for Numerical Methods in Fluids* 1995; **20**:887–913.
35. Nithiarasu P. An efficient artificial compressibility (AC) scheme based on characteristic based split (CBS) method for incompressible flows. *International Journal for Numerical Methods in Engineering* 2003; **56**:1815–1845.
36. Zienkiewicz OC, Nithiarasu P, Codina R, Vázquez M, Ortiz P. The characteristic-based-split procedure: an efficient and accurate algorithm for fluid problems. *International Journal for Numerical Methods in Fluids* 1999; **31**:359–396.
37. Nithiarasu P, Liu CB. Steady and unsteady incompressible flow in a double driven cavity using the artificial compressibility (AC)-based characteristic-based split (CBS) scheme. *International Journal for Numerical Methods in Engineering* 2005; **63**:380–397.
38. Zienkiewicz OC, Taylor RL, Nithiarasu P. *The Finite Element Method for Fluid Dynamics* (6th edn). Elsevier: Amsterdam, 2006.
39. Nithiarasu P. On boundary conditions of the characteristic based split (CBS) algorithm for fluid dynamics. *International Journal for Numerical Methods in Engineering* 2002; **54**:523–536.
40. Nithiarasu P, Zienkiewicz OC, Satya Sai BVK, Morgan K, Codina R, Vázquez M. Shock capturing viscosities for the general fluid mechanics algorithm. *International Journal for Numerical Methods in Fluids* 1998; **28**:1325–1353.
41. Bird RB, Armstrong RC, Hassager O. *Dynamics of Polymeric Liquids*, vol. 1. Wiley: New York, 1977.
42. Rajagopal KR, Ruzicka M. On the modelling of electrorheological materials. *Mechanics Research Communications* 1996; **23**:401–407.
43. Mohyuddin MR, Gotz T. Resonance behaviour of viscoelastic fluid in Poiseuille flow in the presence of a transversal magnetic field. *International Journal for Numerical Methods in Fluids* 2005; **49**:837–847.
44. van Os RGM, Phillips TN. Spectral element methods for transient viscoelastic flow problems. *Journal of Computational Physics* 2004; **201**:286–314.
45. Marchal JM, Crochet MJ. A new mixed finite element for calculating viscoelastic flow. *Journal of Non-Newtonian Fluid Mechanics* 1987; **26**:77–114.
46. Morgan K, Peraire J, Peiro J, Zienkiewicz OC. Adaptive remeshing applied to the solution of a shock interaction problem on a cylindrical leading edge. In *Computational Methods in Aeronautical Fluid Dynamics*, Stow P (ed.). Clarendon Press: Oxford, 1990; 327–344.
47. Hu X, Ding Z, Lee LJ. Simulation of 2D transient viscoelastic flow using the CONNFFESSIT approach. *Journal of Non-Newtonian Fluid Mechanics* 2005; **127**:107–122.

DOI: 10.1002/fld